The Formation of Chondrules: Petrologic Tests of the Shock Wave Model

Harold C. Connolly Jr.

California Institute of Technology

Division of Geological and Planetary Sciences

Mail Code 100-23

Pasadena, CA 91125

and

Stanley G. Love

Jet Propulsion Laboratory

Mail Code 306-438

4800 Oak Grove Drive

Pasadena, CA 91109-8099

Submitted to *Science*

November, 1997

ABSTRACT

Chondrules are mm-sized spheroidal igneous components of chondritic meteorites. They consist of olivine and orthopyroxene set in a glassy mesostasis with varying minor amounts of metals, sulfides, oxides and carbon phases. Their textures and fractionated mineral chemistries suggest that they formed by the repeated, localized, brief (minutes to hours) melting of cold dust aggregates as free floating objects within the protoplanetary nebula. Diverse chondrule formation mechanisms have been proposed over the last century, but none yet explain both the astrophysical and meteoritical observations. In this paper we examine the nebular shock wave model of chondrule formation, focusing on its petrologically observable consequences. We systematically list the most important constraints on chondrule formation and test each one against the shock wave model. We show how the shock wave model agrees remarkably with the most important petrologic and geochemical properties of chondrules. In addition, our model shows how particles within the nebula are size sorted, how rims around chondrules are formed, and how the volatile-rich nature of chondrule rims and unequilibrated chondrite matrix can be explained by the nebular shock wave model.

Primitive meteorites (unequilibrated chondrites, Fig. 1) are generally composed of chondrules, CAI's and matrix material [1]. Of these components, chondrules are usually the most abundant (up to 85 vol%). These mm sized igneous spheres are composed of olivine and orthopyroxene minerals set in a glassy mesostasis with varying minor amounts of metals, sulfides, oxides and carbon phases. The major class of chondrules, ferromagnesian (FeO or MgO-rich, olivine/pyroxene bearing) are divided based on their bulk compositions and textures into two general populations, FeO-poor and FeO-rich [2,3,4 Fig. 2].

Chondrules are convincingly argued to have formed as free-floating objects within non-asteroid/planet body environment(s) during the lifetime of our protoplanetary nebula [3,4,5,6]. Therefore, they are the fossil evidence of processes which operated during the lifetime of our nebula. Although numerous mechanisms for their formation have been proposed [6,7], of the models few have been rigorously tested against the established petrologic and geochemical constraints on chondrule formation [8]. In this paper we expand and then test the nebula shock wave model [9,10] for chondrule formation against the most important constraints for chondrule formation. We begin our study by listing these constraints, then extending and further developing the nebular shock wave model for chondrule formation. Our study ends with a discussion of the results, comparing them against the meteoritic observations.

The Key Petrologic and Geochemical Constraints on Chondrule Origins

1. Chondrule peak temperatures and cooling rates. Studies of natural chondrules and their synthetic analogs have provided valuable constraints on their origins [2,3,4,6,11,12]. Foremost among these constraints are their estimated peak melting temperatures, duration of melting, and cooling rates, all derived from comparisons of textures and fractionated mineral chemistries (mainly variations in FeO and MgO contents) between synthetic and natural chondrules [13,14,15]. Peak temperatures of chondrule formation range from 1700 to 2000°C for durations of seconds to minutes [11,12,13,14,15,16]. The lack of chemically homogeneous minerals within chondrules limits their cooling times to minutes to hours (cooling rates of 100-1000 °C/hr [11,12,13,14,15,17]): more prolonged heating would have facilitated elemental diffusion (equilibration) after crystallization [Fig 2a]. Although the diversity of chondrule compositions and textures prevents unique determination of the temperatures and times of formation for all chondrules, the loss of volatile elements by evaporation provides independent support for the above numbers [18,19].

2. Chondrule precursor temperatures. Another important petrological observation is that some chondrules were relatively cold before they were melted. FeO-poor [Fig 2b], dark-zoned (DZ), and agglomerative olivine (AO) chondrules [Fig. 2c] of unequlibrated chondrites (UC) generally contain sulfide [3,19,20]. Although it has been suggested that

sulfides in chondrules from unequilibrated chondrites are metamorphic products not associated with chondrule precursors [6,8], this has been convincingly argued to be incorrect [19,20]. The presence of sulfide in these chondrules of UC's requires that it was part of their precursors [19,20]. Therefore, because sulfide has an evaporation temperature of ~400°C, preservation of sulfide in the FeO-poor, DZ and AO chondrules requires that they were rapidly heated to their peak melting temperatures from precursors that were resting at an ambient temperature of < ~400oC.

In addition to sulfide, the suggestion [21,22,23] that carbon was present in chondrule precursors, if true, provides an additional constraint on their premelting temperature. Many features of FeO-poor chondrules require one or more carbon phases to have been present within the precursor [22] before melting. If this carbon resided in organic compounds [21], the ambient nebular temperature before chondrules were melted could not have exceeded ~200°C without destroying those compounds.

FeO-rich chondrules do not contain sulfide and likely did not contain either sulfide or carbon within their precursors. However they are rich in moderately volatile elements such as Na and K compared to FeO-poor chondrules [3,4,6,24]. Assuming the majority of Na and K found in these chondrules today is reflective of their precursor components, the precursors of FeO-rich chondrules could not have experienced temperature in excess of ~700°C for extensive periods or the final chondrule observed would contain neither Na or K [6,19].

3. Chondrule recycling. A third important observation is that chondrules have been recycled. Many chondrules contain relict grains

[19,25,26] indicative of earlier generations of chondrules that were formed, broken, reaccreted, and remelted to form new chondrules [6,27,28]. This key observation requires that chondrules experienced many episodes of heating, interspersed with epochs of fragmentation and accretion. Furthermore, the episodic heat pulses varied in intensity. Many chondrules have igneous rims which accreted on existing chondrules as fine-grained, cold dust. Later or concurrent heating events melted these rims without melting the underlying chondrules.

4. Fine-grained dust and chondrule formation. Next, petrologic studies have suggested that chondrules formed in the presence of fine-grained dust. This dust is observed in chondrule rims and is implicated as a seeding mechanism for the crystallization of some chondrules [19,29,30]. Moreover, the chemistries of accretionary rims on chondrules and the matrix material between chondrules may indicate that the dust was intimately involved in the chondrule forming process. A common hypothesis for the origin of volatile-rich dust found in meteorites is that volatile elements evaporated from chondrules during their heating and recondensed on the fine-grained material [29]. This interpretation implies that the dust was present when chondrules were formed, that the dust was less strongly heated than the chondrules, and that chondrules and dust heated together eventually became part of the same meteorite. Another possible origin of volatile-rich matrix material is that it always was volatile-rich, likely representing material which was condensed volatile-rich from the nebular gas. If this is true, and if this material had any relationship to chondrule formation, an important point is that it was still less strongly

heated than chondrules, thus surviving chondrule formation because it was less strongly heated. We would like to point out, however, that we are not implying that all matrix material found in chondrites has been thermal processed during chondrule formation. The presence of interstellar grains (i.e. diamonds and SiC, [31]) requires that at least in part the observed matrix material was not heated to above ~400°C before accretion.

5. Total gas pressure during chondrule formation. Chondrule petrology can place constraints on the total gas pressure under which they formed. Chondrule (FeO-rich and poor) liquids are unstable (will evaporate) under pressures of ~ 10-5 bar (canonical nebula ambient) in a gas of solar composition [32,33]; total pressures of 10-4 to 10-3 are required for liquid stability. To meet this higher pressure requirement, preheated chondrule regions have been modeled to have dust enrichments ranging up to 500X [32] over a gas of solar abundance, with the partial evaporation of dust providing the needed boost to the gas pressure.

6. The fO_2 during chondrule formation. Variations in the chemistry and mineralogy of chondrules suggest that they experienced a range in fO_2 (partial pressure of oxygen, or oxygen fugacity) conditions during their formation [6,21,24]. Unless the inferred fO_2 recorded by chondrules is an artifact of precursor composition [22], FeO-poor chondrules must have formed in an environment with an fO_2 similar to a gas of solar composition whereas FeO-rich chondrules experienced a much higher (by 4-6 orders of magnitude [24]) fO_2. These observations require that if the ambient nebular gas played a role in controlling the redox conditions (i.e. amount of FeO over Fe-metal) of chondrules the partial pressure of oxygen within localized

regions in the nebula was increased by evaporation of dust [32] (and/or ices and tars [34]) significantly enriched compared to a gas of solar composition.

7. Degree of heating and chondrule sizes. Chondrule petrology suggests that their degree of heating may be positively correlated with size. In addition to the possibility (noted above) that fine-grained dust was much less strongly heated than chondrules, DZ and AO chondrules are, in general, smaller than their neighbors. Their textures and sulfide abundances suggest that they are also less strongly heated than other chondrule types. We point out this apparent size dependence while recognizing that better understanding of the relationship between chondrule size and degree of heating would provide a crucial test for any proposed chondrule formation mechanism [35].

8. Formation in localized regions. The last important observation is that chondrules formed in localized regions of the nebula [6]. The relatively rapid heating and slow cooling rates experienced by chondrules constrains their formation to locally hot regions ~100km or smaller in size [36] in the nebula. In addition, there are distinct differences in bulk chemistry and oxygen isotopic composition among chondrules from different meteorites. This result, like the heating duration (and cooling rates) discussed above, implies that the chondrule formation mechanism operated locally, and that its products were not mixed throughout the nebula before becoming incorporated into meteorite parent bodies.

Description of the shock wave model for chondrule formation.

A shock wave is a sharp discontinuity between hot, compressed, high-speed gas (moving faster than the local speed of sound) and cooler, thinner, slower moving gas. Gas overrun by a shock wave is abruptly heated, compressed, and accelerated. We envision the shock as a thin, flat surface (a plane) moving through an initially cool, quiet (turbulent velocities of ~50 m/s [37] or less) nebula of gas and dust. For simplicity, we consider a normal shock, one that travels in a direction perpendicular to its front surface. We assume a cold background nebula temperature T_O of 200 K. The ambient pressure p_o is 1.00×10^{-5} atm. We assume for simplicity that the gas is ideal, diatomic molecular hydrogen (molecular mass m = 3.34×10^{-27} kg/molecule; ratio of specific heats γ=1.4 [38]), so the gas molecule number density (n_o) is 3.7×10^{20} m^{-3} and the gas mass density (ρ_o) is 1.23×10^{-6} kg/m3. The speed of sound (a) in the gas before the shock is given by $(\gamma k T_o / m)^{0.5}$, where k is the Boltzmann constant (1.38×10^{-23} J K^{-1}), and m is the mass of one molecule. It is convenient to express the shock velocity (v_s) in terms of its Mach number (M), the ratio v_s/a If we assume an initial temperature of 200°K, the sound speed is 1100 m/s. Thus, the Mach number is roughly the shock speed in km/s.

Given the Mach number and ideal gas equation of state, analytical relations [38] govern the post-shock density, pressure, velocity, and temperature (ρ_1, p_1, v_1, T_1) in the gas. Typical results for shocks that might form chondrules (M = 3-8, following [9]) are shown in Fig. 3. Temperature

and density increase moderately behind the shock; pressure increases greatly: in a Mach 5 shock, pressure increases by a factor of 29, density by 5, and temperature by 5.8.

Solid particles are also affected by the shock. When a shock overruns them, particles suddenly find themselves in a blast of wind moving at several km/s. Friction (or drag) from collisions of gas molecules heats the particles, as does thermal radiation from hot neighboring particles. Particles lose heat via radiation and evaporation [10,39]. In addition to gas drag heating, particles can also be heated radiatively and conductively by the hot post-shock gas (at 1160°K in the M = 5 example) until cooling begins (40) or a post-shock rarefaction wave (an "inverse shock" that cools and expands the gas) follows.

Once behind the shock, friction with the post-shock gas forces the particles to accelerate to match speeds with it. Drag heating ends when the particles attains the speed of the gas, which occurs when they have encountered a mass of gas comparable to their own mass. This corresponds to a distance behind the shock front on the order of the "stopping distance," $l_{stop} = d_p\rho_p/2\rho_g$, where d_p is the particle diameter, ρ_p is the particle density (2000 kg/m^3 here for uncompacted silicate aggregates), and ρ_g is the post-shock gas density: 6.15×10^{-6} kg/m^3 for the Mach 5 example we treat. Micron-sized particles attain the gas velocity within a few hundred meters of the shock, while mm-sized particles fall hundreds of kilometers behind the shock before matching speeds with the post-shock gas (Table 1). Thus, a transient region of size-sorted particles lies behind

the shock front. Once particles of a given size come up to speed, their number density is concentrated by the same factor as the gas density. Figure 4 is a cartoon illustrating some of these effects.

Comparing the Shock Wave Model with Petrologic Observations: The Test.

1. Chondrule peak temperatures and cooling rates. The shock wave mechanism has consequences that are petrologically observable in chondrites. The first is the intensity and duration of particle heating. Numerous previous studies [9,10] have shown that nebular shocks of Mach 3 to 8 can heat initially cold chondrules (as mandated by the petrologic observations discussed above) to melting temperatures for times consistent with those determined experimentally. In addition to melting, post-shock cooling rates similar to those experienced by chondrules have been determined. We do not reproduce heating intensities or cooling rates here, but wish to emphasize a point not widely discussed in detail by previous models for shock wave heating.

Dissociation of molecular hydrogen [9,35] and evaporative cooling [39] both provide powerful thermostats limiting the peak temperatures of particles in potential stronger shocks to ~1800°C . Curiously, experiments have shown [11,12,13,14,15,16] that the maximum upper temperature limit for chondrule formation is not much above this value (which can increase slightly depending on the total pressure in the shock), thus providing indirect additional support for heating of chondrules in nebular shock waves.

Earlier studies of nebular shock waves have considered primarily heating intensities and times scales. We now go beyond that work, focusing on additional aspects of shock heating which have not been stressed in the existing literature, and which can be tested petrologically.

2. Chondrule precursor temperatures. As discussed above, the presence of sulfides and carbon phases in the precursors of FeO-poor, DZ and AO chondrules suggests that their precursors were rapidly heated to their peak melting temperatures from at a temperatures less than ~400°C. Similarly if FeO-poor and FeO-rich chondrules formed separately, then FeO-rich chondrule could not have experienced temperatures in excess of ~700°C before being melted. Shock wave heating is virtually instantaneous. Once a particle is overrun by the shock wave it is quickly heated to a peak melting temperature (Table 1), thus satisfying the constraint that chondrules were relatively cold before they were heated.

3. Chondrule recycling. The first petrological test of the shock wave model is the notion of chondrule recycling. Because shock waves need not be singular or identical events [7,9,10,41], they can provide the multiple heating episodes of varying intensity indicated by the texture and chemistry of some chondrules. Collisions within shock waves would also have broken up chondrules, assisting in the recycling process.

In our model a chondrule might collide with a particle half its size at half the post-shock gas speed, or 2 km/s in the Mach 5 case discussed above. Such collisions would be relatively rare (assuming a common size spectrum for particles, $n(r,r+dr) \propto r^{-3.5}\, dr$, in which most of the mass is contained in the smallest particles) but would certainly break the

chondrule. This mechanism could create the chondrule fragments seen in chondrites. Chondrule fragments might also supply some of the relict grains observed in recycled chondrules [24,25,26,28,42].

4. A: Fine-grained dust and chondrule formation. Shock wave heating leads to high mutual velocities between particles of different sizes: recall that micron-sized grains stop within a few hundred meters of the shock front, where mm-sized chondrules have not slowed appreciably (Figs. 5 and 6). The resulting velocity mismatch provides opportunities for chondrules to accrete rims of much smaller grains via collisions. In order to match speeds with the post-shock gas flow, a chondrule must encounter a mass of gas comparable to its own mass. The gas colliding with the chondrule carries with it some solid grains. Grains much smaller than the chondrule reach their full post-shock number density close behind the shock (Fig. 5), and collide with the chondrule at maximal relative velocity (Figs. 5 and 6). Particles closer to the chondrule in size have lower number densities and relative speeds. Thus, a chondrule overrun by a shock wave collides preferentially with much smaller particles. Any excess of accreted material on one side of the chondrule would induce rotation [43], ensuring roughly concentric buildup of rim material.

The total mass of small particles which collide with a chondrule overrun by a shock is roughly equal to the chondrule's own mass times the dust/gas ratio of the post-shock nebula. That ratio is the same as the pre-shock value for these small particles over most of the distance required for the much larger chondrule to match speeds with the gas. The canonical nebula dust/gas ratio is ~ 1%. Assuming that the small grains contain a

significant fraction of the solid mass, that their material density is comparable to that of the chondrules, and that they stick efficiently, a chondrule can be expected to accrete about 1% of its own mass in small grains. A 1% change in mass corresponds to 0.3% in radius, or 3 μm for a 1-mm chondrule. This result is consistent with the observed thicknesses of fine-grained accretionary rims on chondrules [44], and with the observation that rim thickness is generally proportional to chondrule radius [44].

Because the accretion of such small grains occurs at the same time as peak drag heating, this mechanism can explain melted, igneous rims on some chondrules. Shocks too weak to melt chondrules could lead to collisional accretion of unmelted fine-grained rims, which are observed on many chondrite constituents [1,19].

A concern with hypervelocity collisional rim accretion is that high-speed impacts might destroy chondrules. For accretion of rim particles smaller than ~ 50 microns, however, the chondrule is likely to survive largely intact, as seen in experimental impacts of mm-sized glass spheres at ~ 5 km/s into porous targets composed of 50 micron glass beads [45]. Fine-grained rims on chondrules are composed of ~ 1-micron grains, whose smaller mass would cause even less damage, especially on a hot, plastic target rather than a cold, brittle one.

B: Volatiles in chondrule rims and chondrite matrix. Chondrule rims and the matrix of chondrites are generally richer in volatile elements than chondrules [19,29]. This observation is consistent with shock wave heating. Fine-grained particles (micron sized) are less strongly heated than chondrules in shock waves because the drag heat pulse duration is

proportional to particle diameter. Weaker heating of smaller particles implies better retention of volatiles. Furthermore, shock heating will actually facilitate the transfer of volatiles from large particles to smaller ones. A 1 mm chondrule experiences its peak heating and evaporation just behind the shock front where it is surrounded by micron sized particles that are no longer being drag heated. These smaller grains are therefore cooler and provide a ready substrate for the condensation of volatiles lost from chondrules.

5. Total pressure during chondrule formation. As noted above, the total gas pressure in the region of chondrule formation appears to have been 10 to 100 times higher than the canonical nebula midplane value [ ]. Figure 3 shows that shocks strong enough to melt chondrules are accompanied by gas pressure increases of 10 to 74 times the preshock value. Shock heating thus explains both chondrule melting and its apparent high pressure environment with a single mechanism.

6. The fO_2 during chondrule formation. Related to pressure is the fO_2 which chondrules experienced during formation. FeO-poor chondrules likely experienced fO_2 conditions similar to the ambient nebula, while FeO-rich chondrules formed under much more oxidizing conditions [6]. Variable fO_2 has been explained by the evaporation of fine dust in different concentrations [6,32]. Such a model, however, cannot by itself explain the stability of FeO-poor chondrule liquids because the dust concentration required to explain the inferred fO_2 value is not high enough to raise the total gas pressure enough to stabilize the liquid. In shock wave heating, however, pressure is not necessarily correlated with dust concentration,

permitting chondrule liquids to be stable under a wide range of fO_2. Thus shock wave heating resolves the paradoxical fO_2 values inferred from FeO-poor chondrules.

7. Degree of heating and chondrule sizes. The shock waves model can also explain the difference in degree of heating between FeO-rich and FeO-poor chondrules. In general FeO-rich chondrules experienced more heating [12] and higher fO_2 than FeO-poor chondrules. In general, stronger shocks produce higher drag heating temperatures, higher post-shock total gas pressure and more particle evaporation resulting in higher fO_2. Thus FeO-rich chondrules may be the product of shocks stronger than those that produce FeO-poor chondrules.

Alternatively, FeO-rich and FeO-poor chondrules may have been formed together. FeO-rich chondrules are generally larger than FeO-poor chondrules [3,4]. Their greater size implies a proportionally larger stopping distance and a correspondingly longer drag heat pulse duration in the same shock wave (Table 1). The longer heat pulse would produce more strongly heated chondrules. In this scenario the larger FeO-rich chondrules would be more oxidized than FeO-poor chondrules because of longer interaction with the post-shock gas or differences in precursor composition. Note that the correlation between particle size and degree of heating in shock waves is consistent with DZ and AO chondrules being both the smallest and least heated of all chondrule types.

8. Formation in localized regions. The last important property of chondrule formation that we will discuss is their production in localized regions and variability across meteorite types. As discussed earlier, many

lines of evidence (i.e., cooling rates of chondrules, oxygen isotopes) suggest that chondrule formation occurred in localized regions of the nebula. Shock waves satisfy this constraint because their lateral size and the distance they travel (and hence the distance they carry particles) may have almost any value, depending on the mechanism that generates them. The only requirement that the present model levies on the spatial scale of shocks is that they travel several hundred kilometers, far enough to produce the particle size-sorting behavior discussed above. This distance easily meets the petrologic constraint that the nebula not be homogenized before the meteorite parent bodies accreted.

Sources of nebular shocks. We have shown that shock wave heating agrees remarkably well with all of the most important observed properties of chondrules. The shock wave model suffers, however, from a major uncertainty needing mention here. As summarized by [7] strong shocks dissipate rapidly and require great energy (~10% of the energy of gravitational binding to the sun for a chondrule-forming shock at 2-3 AU) to form. Thus, it is important to identify a powerful, reliable, repeatable, and astrophysically realistic source for the shocks. No such source has been positively identified and observed. Although it is beyond the scope of this paper to treat in detail potential shock formation mechanisms, we note that three processes capable of creating chondrule-forming shocks have been proposed and investigated in recent years. These are irregular (clumpy) accretion of interstellar gas onto the protoplanetary nebula [7,10, 45] outbursts from the young Sun (analogs of FU Orionis events) [7], and spiral arm instabilities in the disk [7,47, 48]. Direct detection of these

mechanisms operating in protoplanetary disks is beyond the capability of current astronomical techniques. Nevertheless, we believe that the existence of several candidate shock-forming processes, along with the superb match between the properties of chondrules as predicted for shock wave heating and as observed in meteorites, provides strong evidence for chondrule formation in nebular shocks.

REFERENCES

1. D. W. Sears and R. T. Dodd, in *Meteorities and the Early Solar System*, J. F. Kerridge and M. S. Mathews, Eds. (Univ. of Arizona Press, Tucson, 1988), pp. 3-31.

2. E. R. D. Scott and G. J. Taylor, *Proc. Lunar Planet. Sci. Conf.* **14** B275-86 (1983).

3. R. H. Jones and E. R. D. Scott, *Proc. Lunar Planet. Sci. Conf.* **19th** pp. 523-36 (1989); R. H. Jones *Geochim. Cosmochim. Acta.* **58**, 5325-40 (1994).

4. R. H. Jones, *Geochim. Cosmochim. Acta.* **54**, 1785-1802 (1990); R. H. Jones, *Geochim. Cosmochim. Acta* **60**, 3115-38 (1996).

5. G. J. Taylor, E. R. D. Scott, K. Keil, in *Chondrules and their Origins*, E. A. King Ed. (Lunar and Planetary Science Institute, Houston, TX, 1983) pp. 262-78.

6. J. N. Grossman, in (1) pp. 680-96.

7. A. P. Boss in *Chondrules and the Protoplanetary Disk* R. H. Hewins, R. H. Jones, E. D. R. Scott, Eds. (Cambridge Univ. Press, 1996) pp. 257-64.

8. R. H. Shu, H. Shang, T. Lee *Science* **271**, 1545-1551 (1997).

9. L. L. Hood and M. Horanyi, *ICARUS* **93,** 259-69 (1993).

10. L. L. Hood and D. A. Kring, in (7) pp. 265-276.

11. G. E. Lofgren, in (7) pp. 187-96.

12. R. H. Hewins, *Annu. Rev. Earth Plan. Sci.* **25** 61-83 (1997); R. H. Hewins and H. C. Connolly Jr. in (7) pp.197-204.

13. G. E. Lofgren , *Geochim. Cosmochim. Acta* **53** 461-470 (1989).

14. G. E. Lofgren and A. Lanier, *Geochim. Cosmochim. Acta* **54** 3537-3551 (1990).

15. P. M. Radomsky and R. H. Hewins, *Geochim. Cosmochim. Act.* **54** 3475-3490 (1990).

16. H. C. Connolly Jr., B. D. Jones, R. H. Hewins *Geochim Cosmochim. Acta*. in revision.

17. R. H. Jones and G. E. Lofgren, *Meteoritics* **28**, 213-21 (1993).

18. Y. Yu and R. H. Hewins, *Geochim. Cosmochim. Acta.* in revision. (1998).

19. Y. Yu., R. H. Hewins, B. Zanda, in (7) pp. 213-19; M. K. Weisberg and M. Prinz in (7) pp. 119-127.

20. B. Zanda, Y. Yu, M. Bourot-Denise, R. H. Hewins, *LPI Technical Report* **97-02** Part 1, pp. 68-70.

21. J. A. Wood, *Earth Planet. Sci. Lett.* **70**, 11-26 (1984).

22. H. C. Connolly Jr., R. H. Hewins, R. D. Ash, B. Zanda, G. E. Lofgren, *Nature* **371** 136-39 (1994).

23. P. Hanon, F. Robert, M. Chaussidon, *Meteoritics* **31**, A57 (1996).

24. J.N. Grossman, A. E. Rubin, H. Nagahara, E. A. King in (1), pp. 619-59.

25. H. Nagahara, *Nature* **292**, 135-36 (1981).

26. E. R. Rambaldi, *Nature* **293**, 558-61 (1981).

27. C. M. O'D. Alexander in (7), pp. 233-42.

28. R. H. Jones and L. R. Danielson, *Meteoritics and Planetary Science* **32**, 753-60, (1997).

29. E. R. D. Scott, D. J. Barber, C. M. Alexander, R. Hutchison, J. A. Peck in (1), pp. 718-745.

30. H. C. Connolly Jr. and R. H. Hewins *Geochim. Cosmochim. Acta.*, **59** 3231-46 (1995).

31. G. R. Huss in *Astrophysical Implications of the Laboratory Study of Presolar Materials,* T. J. Bernatowicz and E. Zinner Eds. (American Institute of Physics, 1997) pp. 721-48.

32. D. S. Ebel and L. Grossman, *Lunar Planet. Sci. Conf.* **28th,** pp. 317-18 (1997)., D. S. Ebel and L. Grossman, *Meteoritics and Planet. Sci.* **32**, A36-7 (1997).

33. Y. Yu and R. H. Hewins, *Lunar Planet. Sci. Conf.* 28,1613-14 (1997).

34. J. A. Wood and A. Hashimoto, *Geochim. Cosmochim. Acta.,* **57**, 2377-88 (1993).

35. E. R. D. Scott, S. G. Love, A. N. Krot in (7), pp. 87-98.

36. D. L. Sahagian and R. H. Hewins, *Lunar Planet. Sci.* **23**, 1197-98 (1992).

37. J. N. Cuzzi, A. R. Dobrovolskis, R. C. Hogan in (7), pp. 35-44.

38. H. W. Liepmann and A. Roshko, *Elements of Gasdynamics*, (John Wiley and Sons, New York, 1957) 439pp.

39. S. G. Love and D. E. Brownlee, *ICARUS*, **89** 26-43 (1991).

40. T. V. Ruzmaikina and W. H. Ip, *ICARUS*, **112** 430-47 (1994); T. V. Ruzmaikina and W. H. Ip in (7) pp. 277-284.

41. P. Cassen in (7) pp.21-28.

42. G. E. Lofgren, *Lunar Planet. Sci. Conf.* **28**, pp. 827-28; G. E. Lofgren in (20) pp. 40-42.

43. K. Liffman and M. J. I. Brown in (7), pp. 285-302.

44. J. M. Paque and J. N. Cuzzi, *Lunar. Planet. Sci. Conf.* **28**, 1071-72 (1997).

45. S. G. Love, F, Horz, D. E. Brownlee *ICARUS* 105, 216-24 (1993).

46. A. P. Boss and J. A. Graham, *ICARUS* **106**, 168-78 (1993).

47. G. Morfill, H. Spruit, E. H. Levy in Protostars and Planets II E. H. Levy and J. I. Lunine, Eds. (University of Arizona Press, 1993), pp. 939-978.

48. J. A. Wood, *Meteoritics and Planet. Sci.* **31**, 641-46.

49. We would like to thank Drs. P. Cassen, D. Woolum, D. Burnett, T. Ahrens, R. Ash, G. Huss and S. Russell for their numerous helpful discussions and support on this project. This work was supported by NASA grant. Division Contribution number 8507.

Figure Captions

Figure 1. A transmitted light image of a thin section of Semarkona (LL3.0), an unequilibrated ordinary chondrite. This "holy grail" meteorite has experienced virtually no thermal metamorphism and thus contains chondrules that likely preserve a record of the preaccretional environment within the nebula where they formed. Note the diversity of the chondrules (the round objects), their various sizes, shapes and textures. For scale the large chondrule in the upper right is~3mm by 2mm.

Figure 2. These are three backscatter electron images of chondrules from thin sections. The variation in color correspond to variation in atomic number within each mineral or phase. For example the dark gray in the center of the grains in 2A corresponds to enrichments in MgO but depletions in FeO, however the lighter color gray corresponds to depletion in MgO and enrichments in FeO. The small in the upper right corner is a magnified view of each chondrule which shows the differences in grain sizes. Please note that the scale bars differ for each image and magnified area are all different. (a) A large, FeO-rich, olivine-rich, chondrule from the ALH77176,17 (L3.2) Antarctic meteorite. FeO-rich chondrules are generally larger than FeO-poor chondrules, contain abundant glass and

minerals with a fractionated chemistry (moderately rapid growth from a liquid). They are also typically fragmented. Prolonged heating after formation, depending on the temperature and time of heating, would recrystallize the glass and homogenize the olivine grains. Clearly this is not the case for most FeO-rich chondrules in unequilibrated ordinary chondrites and provides a valuable constraint on their formation. (b) A FeO-poor, olivine-rich chondrule from Semarkona (LL3.0). These chondrules are generally smaller than the FeO-poor chondrules. They contain varying amounts of sulfide and metal (bright white colored phase) and have a smaller silicate grain size. This particular chondrule contains relict dusty olivine grains, observed in the magnified area in the upper right corners. These relict grains are testament to the recycling of chondrules. Their disequilibrium with surrounding grains suggests that they originally formed within another chondrule. In general the textures of FeO-poor, olivine-rich chondrules indicates that they have been melted and heated less than FeO-poor chondrules. C: An agglomeratic olivine chondrule from Semarkona (LL3.0). Note the abundant sulfide and Fe-rich metal (bright white phase). In general these are the smallest, least heated and least melted of all chondrule types. The magnified view shows how fine-grained these objects are (note scale bar is 10μm). An area relatively free of opaque minerals was selected to illustrated the grain size of the silicates and the presence of glass, suggesting that these objects have been partially melted, but only slightly compared to other chondrules.

Figure 3. Post- to pre-shock pressure, temperature, and gas density ratios as a function of shock strength expressed in Mach number. Shocks of Mach 3 to 8 are thought capable of forming chondrules. A Mach 5 shock increases the density by factor of 5, the temperature by a factor of 5.8, and the pressure by a factor of 29.

Figure. 4. Cartoon illustrating a shock wave in dusty gas, drawn from the perspective of an observer moving alongside the shock. Ambient nebular gas with pressure p_0, density ρ_0, and temperature T_0 enters the shock wave at the shock propagation speed v_s. The shock sharply (in the ideal case instantaneously) compresses and heats the gas to higher pressure p_1, density ρ_1, and temperature T_1 while slowing its speed to v_1; the lost kinetic energy powers the heating and compression. Solid particles entering the shock abruptly find themselves in a hot, high-pressure wind with velocity (v_s-v_1). Collisions with gas molecules heat the particles while damping their velocity relative to the gas. Most of a particle's velocity is lost when it has penetrated one stopping distance ($l_{stop} = d_p\rho_p/2\rho_g$) past the shock front. The time scale of this process--and of the gas drag heat pulse--is $L_{stop}/(v_s-v_1)$. Small particles match speeds with the post-shock gas promptly (~ 200m and ~ 0.05s past shock passage for a 1 micron grain in our "reference" Mach 5 shock). Larger particles take proportionally longer to come up to speed (e.g., ~ 200km and ~ 50s for a 1-mm chondrule). A large particle suffers collisions with smaller grains moving at the speed of the gas just behind the shock._The final space density of solids (after matching speeds with the

post-shock gas) is related to the pre-shock value by the same ratio as the gas density (ρ_1/ρ_0).

Figure 5. Relations for particles of density 2 g/cm^3 overrun by a Mach 5 shock in a nebula with ambient pressure of 1e-5 atm and ambient temperature of 300 K. (a) Velocity with respect to the post-shock gas as a function of distance behind the shock for particles 1 μm, 30 μm, 1 mm, and 3 cm in diameter, normalized to the post-shock gas speed (0.8 times the shock velocity for a Mach 5 shock). Velocities are approximated by $v = v_0 e^{-x/l_{stop}}$, where v_0 is the initial speed relative to the gas, x is the distance behind the shock, and l_{stop} is the stopping distance in the post-shock gas. The stopping distance is given by $l_{stop} \approx d_p \rho_p / 2\rho_{gas}$, where d_p is the particle diameter and ρ_p and ρ_{gas} are the particle and gas densities, respectively. For reference, the stopping distances for 1 μm and 1 mm particles in the present case are respectively 200 m and 200 km. The transient velocity sorting of particles according to size is evident. (b) Particle number density enhancement relative to the pre-shock value as a function of distance behind the shock for particles 1 μm, 30 μm, 1 mm, and 3 cm in diameter. The asymptotic value is equal to the post- to pre-shock gas density ratio. Particle number densities are temporarily segregated according to size behind the shock.

Figure 6. Contours of mutual particle collision speeds, expressed as a fraction of the post-shock gas velocity v_1 at 1 km (lower right half of plot) and 1000 km (upper left half of plot) behind the shock wave described in the caption of Fig. 5. The logarithms of the diameters of the two collision partners (in meters) define a point on the contour plot from which the mutual collision speed can be estimated. Two different distances can be shown because the contours for each are symmetric under exchange of the two particle diameters. The figure shows, 1 km behind the shock a 10 μm particle and a 100 μm particle collide at ~ 0.35 times the postshock gas speed, whereas 1000 km behind the shock a 1 cm particle and a 10 μm particle collide at ~ 0.60 times the postshock gas speed.

Table 1. Drag heat pulse durations for different-sized particles in shocks of different strength.

Mach	1μm	100μm	300μm	1mm	2mm	1cm
4	55ms	5.5s	16.5s	55s	110s	550s
5	40ms	4.0s	12.0s	40s	80s	400s
6	32ms	3.2s	9.6s	32s	64s	320s
7	26ms	2.6s	7.8s	26s	52s	260s
8	22ms	2.2s	6.6s	22s	44s	220s

These are calculated by dividing the stopping distance by the shock velocity, giving an order-of-magnitude estimate of the drag heat pulse duration. These calculations assume a pre-shock pressure of 10^{-5} atm and pre-shock temperature of 300°K.

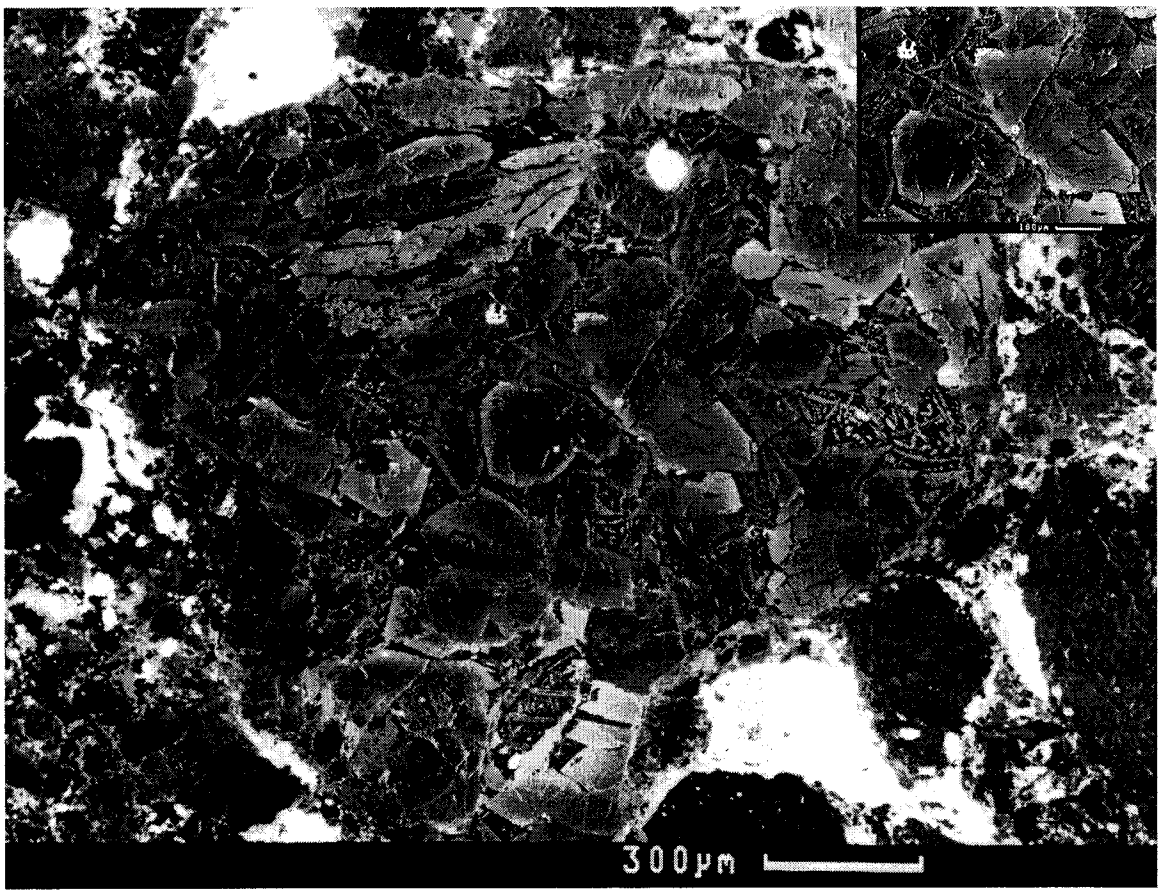
300μm

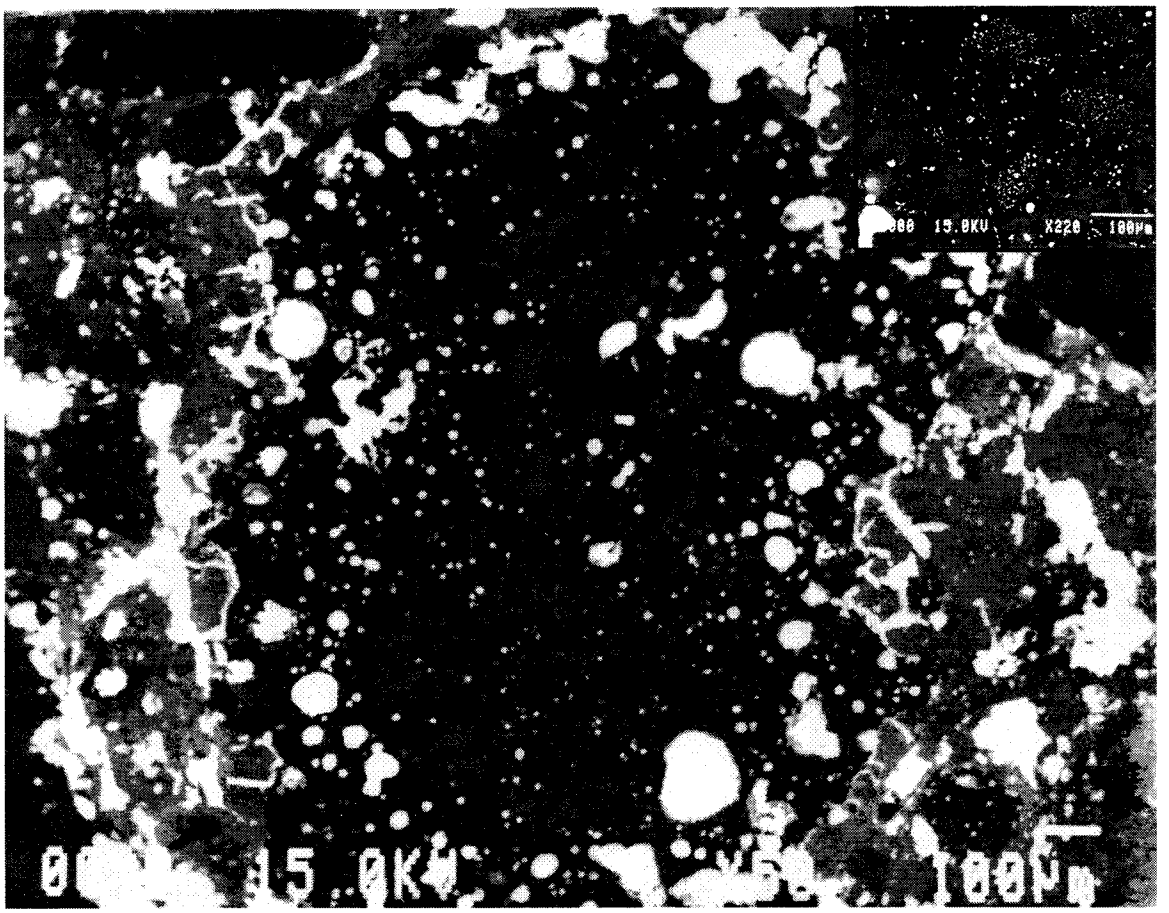
15.0KV
X220
100µm

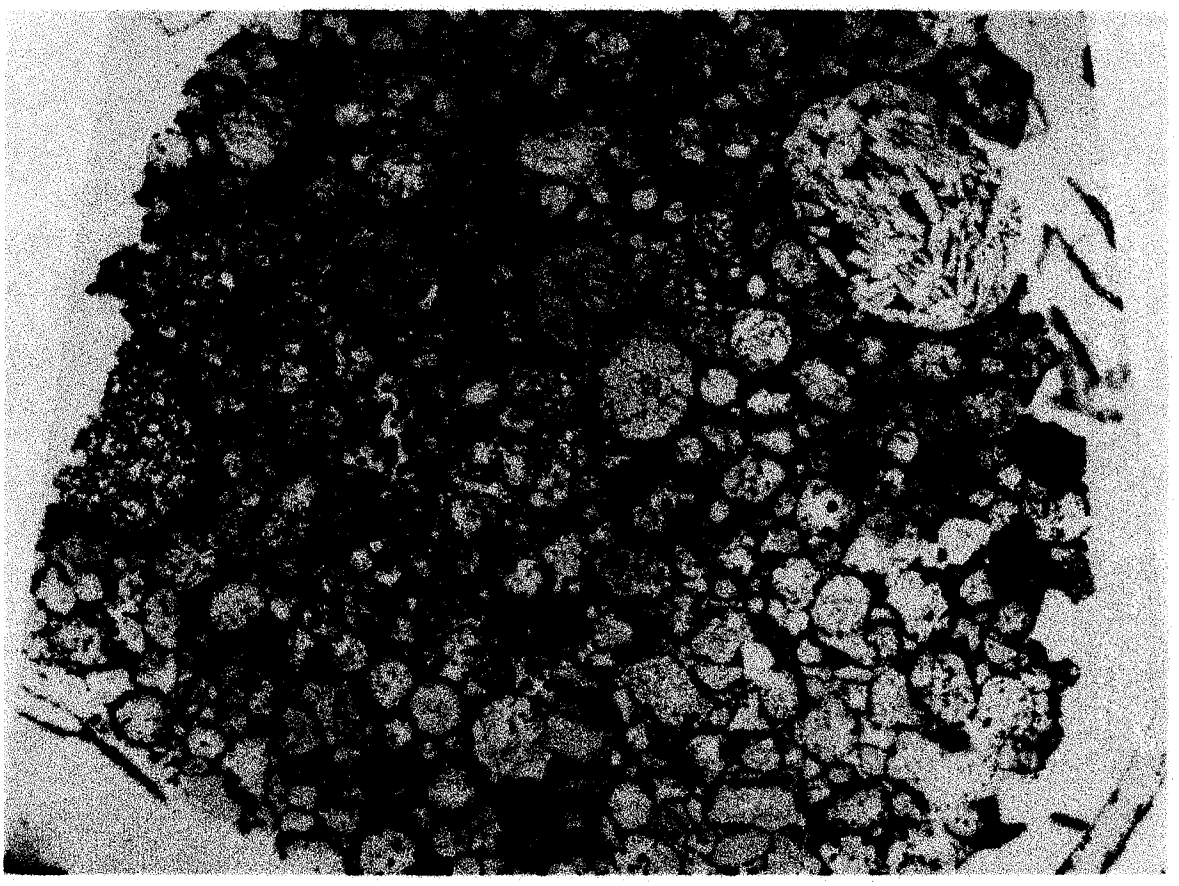

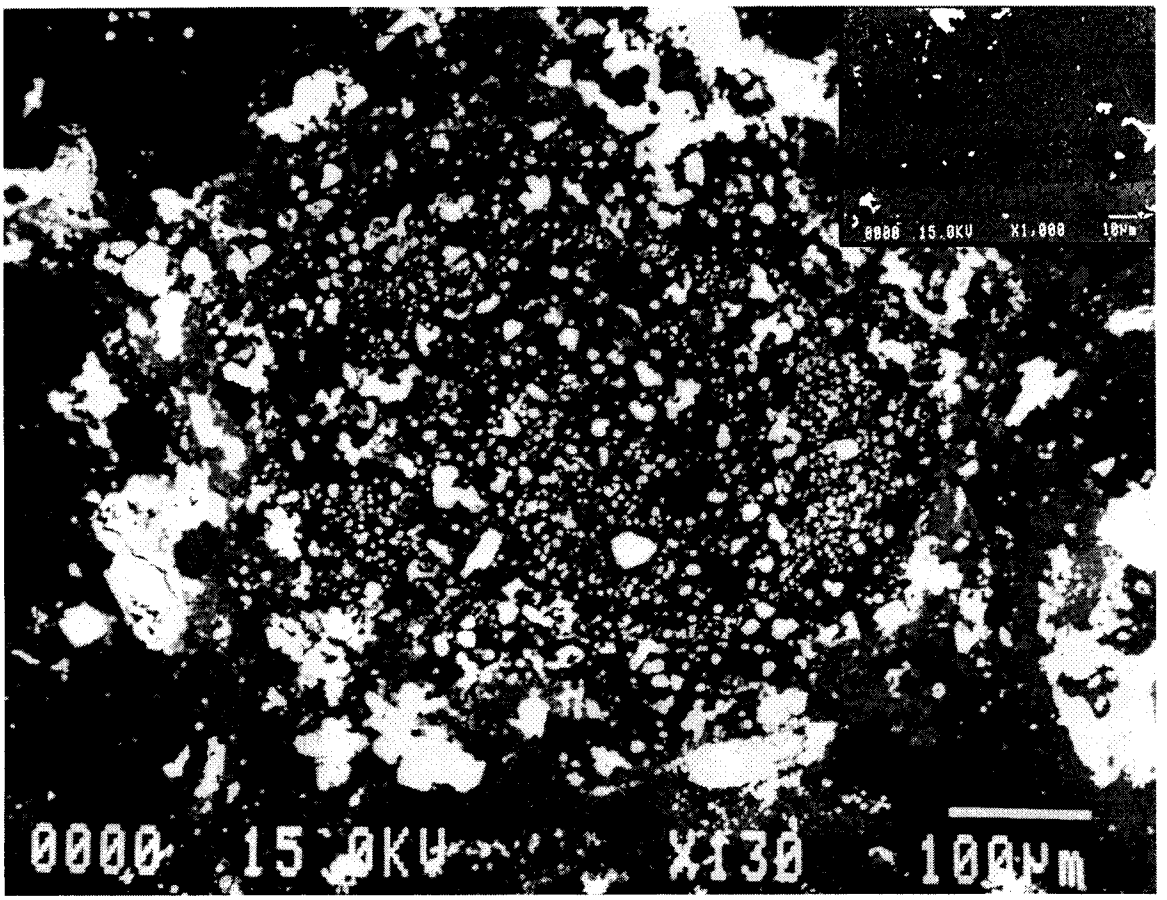
0000 15.0KV X1,000 10μm
0000 15.0KV X130 100μm

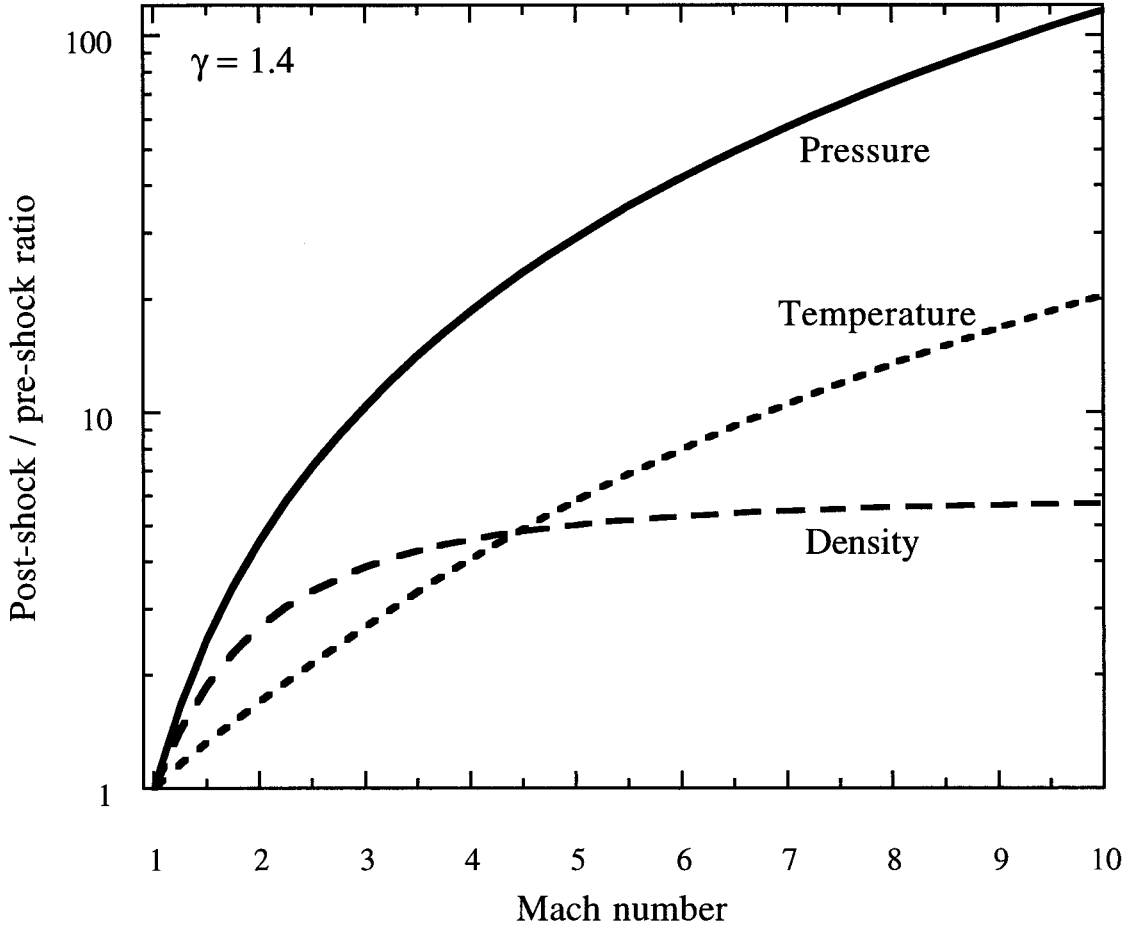

Connolly & Love

Figure 3

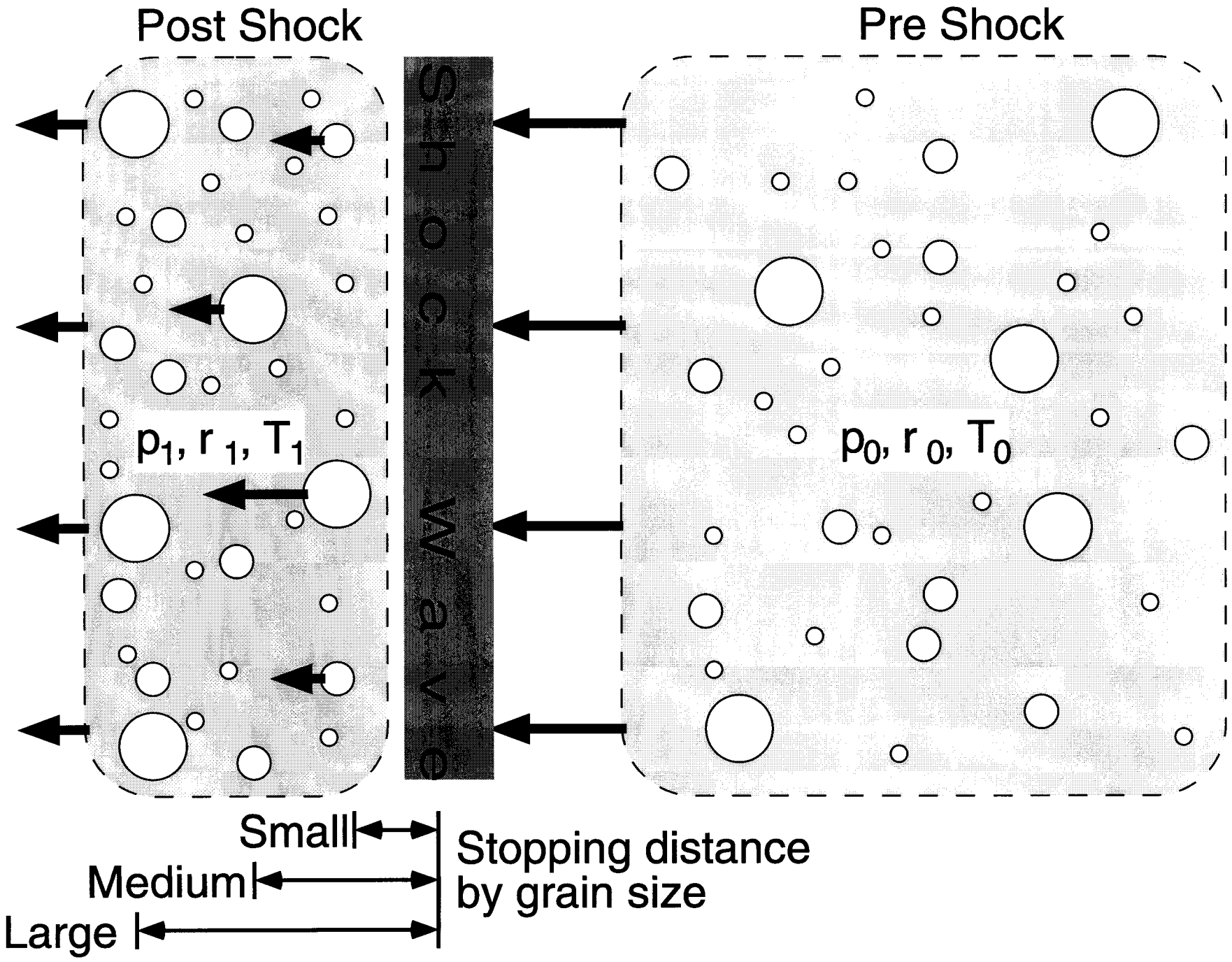

Connolly & Love

Figure 4

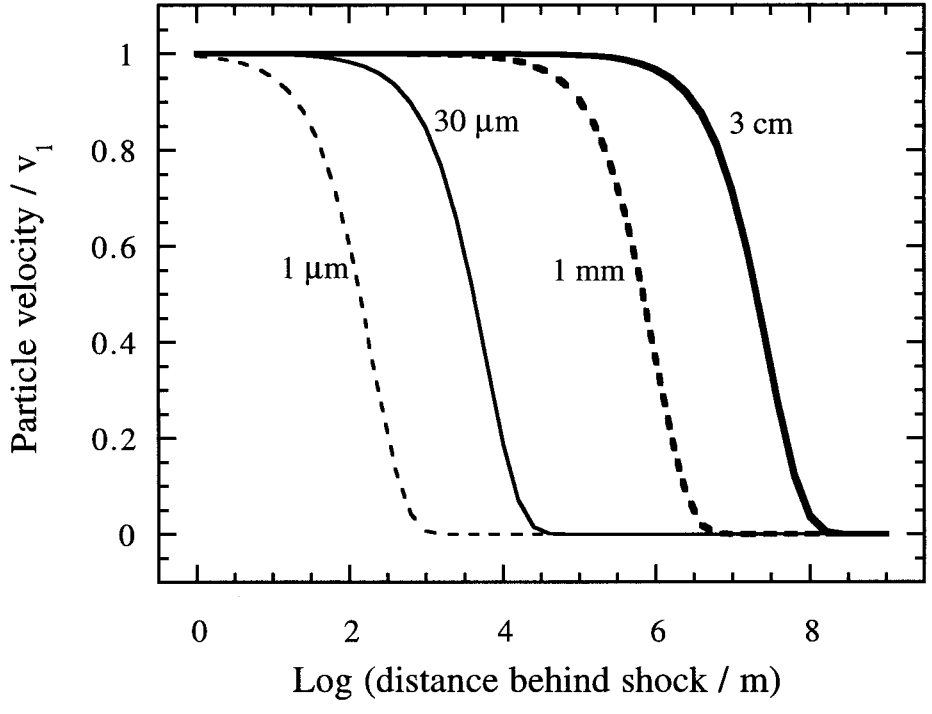

Connolly & Love

Figure 5a

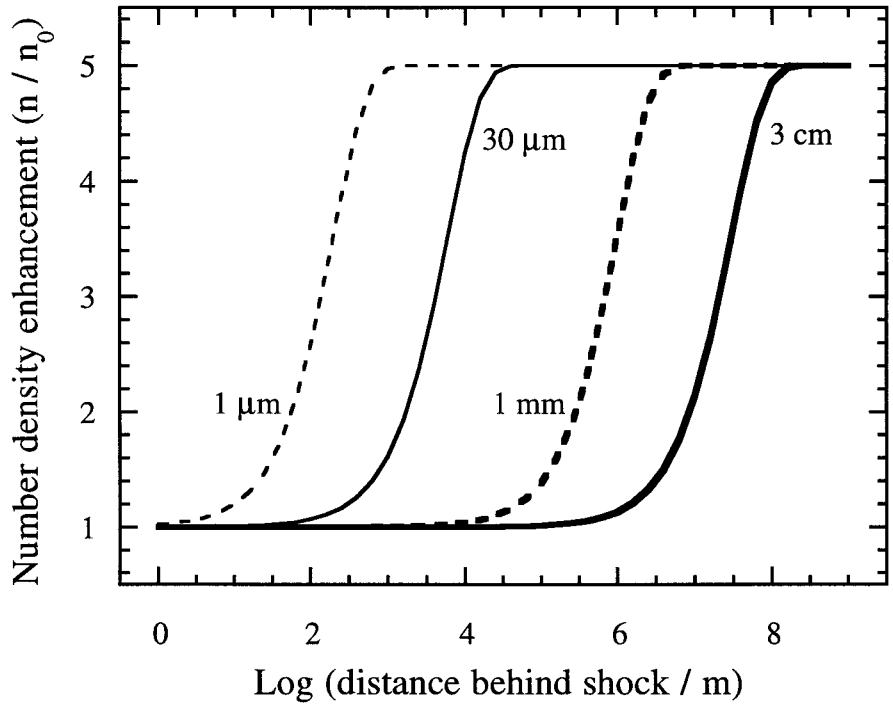

Connolly & Love

Figure 5b

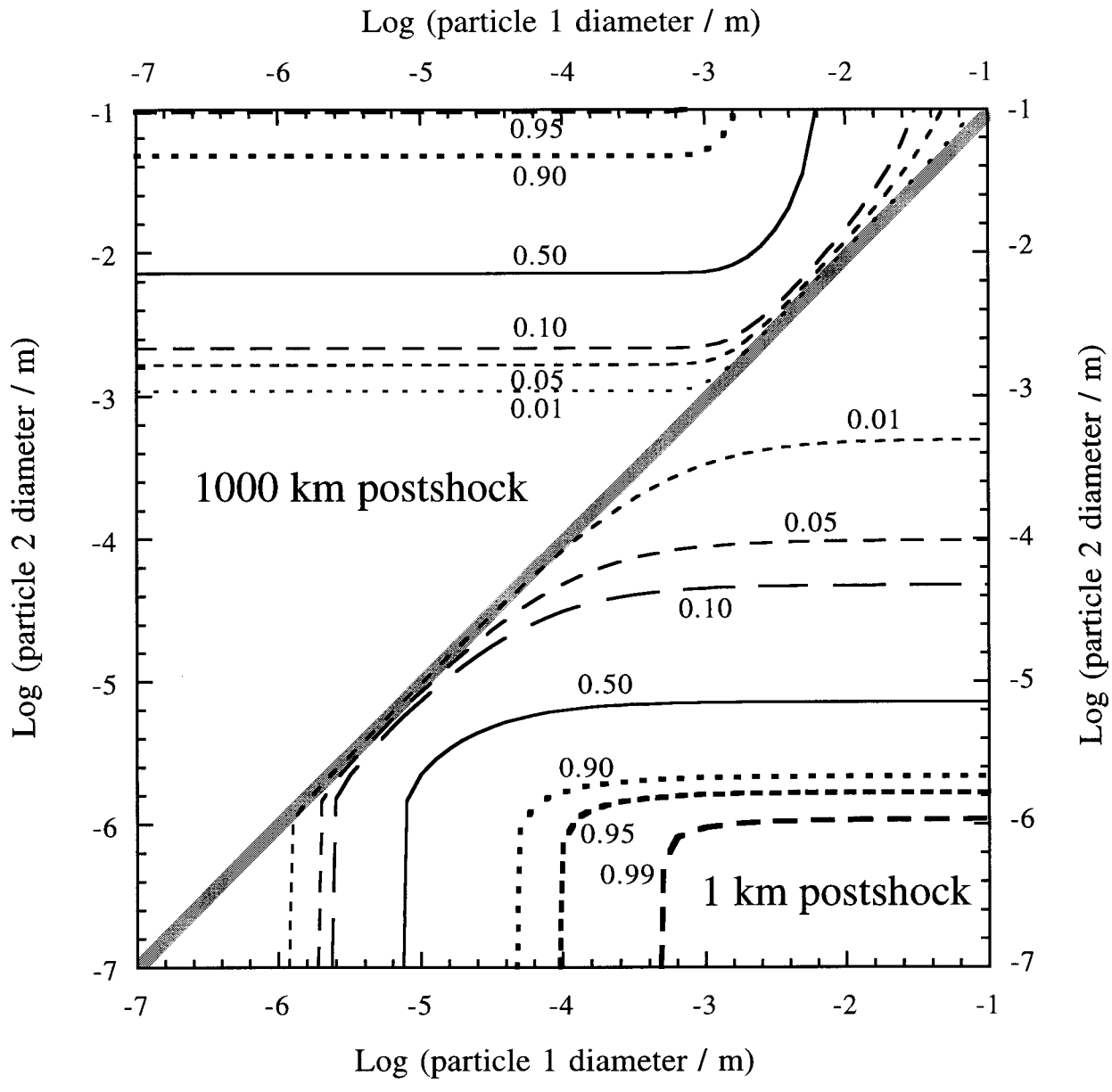

Connolly & Love

Figure 6